ISSN 2630-0958

Journal de Physique de la Soaphys

J. P. Soaphys

Volume 2, Numéro 2 - Décembre 2020

SOAPHYS©

Journal de Physique de la Soaphys
Volume 2, Numéro 2, Décembre 2020

Journal de Physique de la Soaphys
Volume 2, Numéro 2, Décembre 2020

SOMMAIRE

J. P. Soaphys, Vol 2, N°2 (2020) C20A28
http://dx.doi.org/10.46411/jpsoaphys.2020.02.28

Journal de physique de la SOAPHYS
http://www.soaphys.org/journal/
ISSN Print : 2630-0958

THEORETICAL AND EXPERIMENTAL ANALYSIS OF A BOOST CONVERTER

Badiane Modou [1, *], Honadia Prince Abdoul Aziz [2], and Barro Fabé Idrissa[3]

[1] *Semiconductors and Solar Energy Laboratory, Department of Physics to the Faculty of Science and Technique, Cheikh Anta Diop University, Dakar, Senegal, modoubadiane99@gmail.com .*
[2] *Thermal and Renewable Energies Laboratory, Department of Physics to Polytechnic University Center of kaya, Burkina Faso, prince13462@yahoo.f r.*
[3] *Semiconductors and Solar Energy Laboratory, Department of Physics to the Faculty of Science and Technique, Cheikh Anta Diop University, Dakar, Senegal, fabe.barro@ucad.edu.sn.*

INFOS SUR L'ARTICLE

Historique de l'article:
Reçu le : 24 novembre 2020
Réçu en format revisé le : 22 mars 2021
Accepté le : 12 mai 2021

Keywords : *Duty cycle, gain factor, efficiency, ESR, power losses*

Mots-Clés : *Rapport cyclique, gain en tension, rendement, ESR, pertes de puissance.*

ABSTRACT

Abstract: A theoretical and experimental study of a conventional boost converter is presented. Based on the real behavior of the components, the conventional boost converter model dealing with both inductive and capacitive losses as well as switching losses is introduced. From this model, the detailed analytical expressions of the voltage gain factor and the conversion efficiency are established taking into account the losses due to parasitic resistances and switching losses. The behavior of the converter is then analyzed by simulating the voltage gain factor and the conversion efficiency as a function of the duty cycle. The converter prototype was manufactured and a set of experimental measurements was made; these measurements made it possible to demonstrate that the proposed theoretical models were reliable for a large range of duty cycle for the boost converter.

RESUME

Une étude théorique et expérimentale d'un convertisseur boost conventionnel est présentée. Sur la base du comportement réel des composants, le modèle de convertisseur élévateur traitant aussi bien des pertes inductives et capacitives que des pertes de commutation est introduit. À partir de ce modèle, les expressions analytiques détaillées du facteur de gain en tension et du rendement de conversion sont établies en tenant compte des pertes dues aux résistances parasites et aux pertes de commutation. Le comportement du convertisseur est ensuite analysé par simulation du facteur de gain en tension et du rendement de conversion en fonction du rapport cyclique. Le prototype du convertisseur a été mis en œuvre et un ensemble de mesures expérimentales a été effectué ; ces mesures ont permis de démontrer que les modèles théoriques proposés étaient fiables pour une large gamme de rapport cyclique du convertisseur boost.

I. INTRODUCTION

Nowadays the human has become aware of the climatic damage caused by most of the energy sources it uses every day. To counter this, clean energy sources are increasingly in demand, leading to the development of new or alternative energy technologies. These alternative energy technologies are essentially renewable energies. Renewable sources such as solar photovoltaic (PV) and wind power are increasingly being used due to environmental concerns and advances in technology and rapidly decreasing manufacturing costs Kesraoui et al.,2011; Shuhui et al.,2011

However, renewable energy sources have low output voltage characteristics. Therefore, electronic power converters are generally used to convert the output power of photovoltaic panels to match the load demand to improve the dynamic and static characteristics of green generation systems. This is particularly true in the case where a microinverter is provided to each PV module of solar PV systems Wang et al.,2013; Ternifi et al.,2017; Variathet al.,2010; Li et al.,2008; Haibing et al.,2011; Petreuş et al.,2013. Such a microinverter typically consists of two stages; the first stage uses the high step-up DC-DC converter to meet the voltage demand of the second stage and also acts as a maximum power point follower in order to obtain maximum power from the PV module. The second stage is a DC-to-AC inverter to meet the load demand.

Many high step-up DC-DC converters have been designed Li et al.,2009; Wu et al.,2018; Taghvaee et al.,2013; Wu et

al.,1997 with advantages and disadvantages, but all are derived from the conventional boost converter Ayop et al.,2018; Winder et al., 2017; Dash et al.,2015; Abosorrah et al.,2013; Wu et al.,2016; Sadek et al.,2015.

The conventional boost has many disadvantages such as high voltage stress across the switching device. Indeed, its performance is limited due to a higher state resistance leading to more conduction losses in the switch, losses in the leakage inductance, parasitic capacitance Erickson et al.,2004; Das et al.,2012; Rajesh et al.,2015; Mahela et al.,2017.

These drawbacks are the major limitation in the use of this type of converter; thus, it is important to know exactly how the different components affect the performance of the converter and what is the contribution of resistive and switching losses to each other and to the total losses in the converter. Based on this loss model, this study will present a detailed mathematical formulation of the voltage gain factor and conversion efficiency for a conventional boost. Simulations are then carried out to show the effects of the different losses but also to quantify these losses compared to the ideal model. Finally, a design and the realization of a prototype of the converter will be proposed in order to carry out a set of experimental measurements which will allow us to demonstrate that the proposed theoretical model is reliable.

II. MODELING, MATHEMATICAL FORMULATION AND APPLICATION

2.1 Modeling and mathematical formulation

The studied converter is presented on *figure. 1*; assuming that all components are ideal and the converter is operating in Continuous Conduction Mode (CCM) Durán et al.,2011 as this operating mode is more suited for photovoltaic applications, the basic equations are as follows Branko et al.,2015:

$$v_L = L\frac{di_l}{dt} = \begin{cases} V_{in} & 0 < t < \alpha T \\ V_{in} - V_0 & \alpha T < t < T \end{cases} \quad (1)$$

$$V_0 = \frac{V_{in}}{(1-\alpha)} \quad (2)$$

with α being the steady state duty cycle and T the switching period.

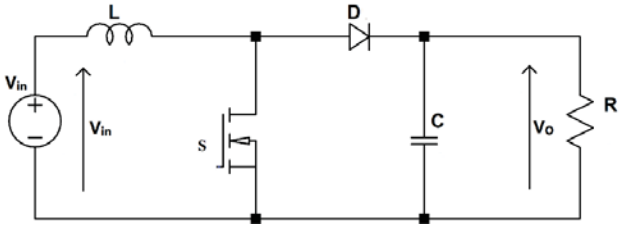

Figure 1: Ideal model of the boost converter.

The model presented above did not take into account the resistive losses through inductor and capacitor and the switching losses through active components (the Mosfet T and the diode D). The following model in *figure2* of the converter do take into account these losses.

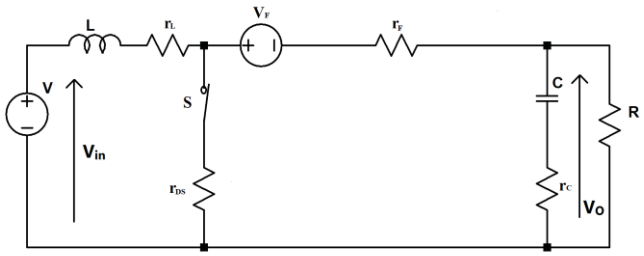

Figure 2: Boost converter with series losses and switching losses.

The power balance for the converter is:

$$P_I = P_0 + P_{r_L} + P_{r_C} + P_{FET} + P_D \quad (8)$$

P_{FET}, P_D are respectively the power losses though the switch T and the diode D.

After some mathematical manipulations, we obtain Honadia et al.,2018:

$$V_{in}\cdot\frac{V_0}{(1-\alpha)R} = \frac{V_0^2}{R} + r_L\cdot\frac{V_0^2}{(1-\alpha)^2R^2} + r_C\cdot\frac{\alpha V_0^2}{(1-\alpha)R^2} + \frac{\alpha r_{DS}V_0^2}{(1-\alpha)R^2} + \frac{1}{2}f_S C_0 V_0^2 + \frac{r_F V_0^2}{(1-\alpha)R^2} + \frac{V_F V_0}{R} \quad (9)$$

R, r_L,r_C, are respectively the load resistor, inductive and capacitive resistance; f_S, r_{DS}, C_O are the transistor switching frequency, on resistance and output capacitance; r_F and V_F are the diode dynamic resistance and forward voltage.

The voltage gain factor G is then deduced as :

$$G = \frac{(1-\alpha)R}{(1-\alpha)R^2 + r_L + r_C\alpha(1-\alpha) + r_{DS}\alpha + 1/2\, f_S C_0 (1-\alpha)^2R^2 + \frac{V_F}{V_0}(1-\alpha)^2R + R_F(1-\alpha)} \quad (10)$$

For the conversion efficiency, we have Honadia et al.,2018:

$$\eta = \frac{P_0}{P_0 + P_{r_L} + P_{r_C} + P_{FET} + P_D} \quad (11)$$

This leads to:

$$\eta = \frac{1}{1 + \frac{\alpha r_{DS} + r_L}{(1-\alpha)^2 R} + \frac{r_F + \alpha r_C}{(1-\alpha)^2 R} + \frac{V_F}{V_0} + \frac{1}{2} f_S C_0 R} \quad (12)$$

2.2 Application

a. Design

The classic boost has been sized according to the following specifications:

An input voltage of 12V for an output voltage of 30V and an output current between 0.5A and 2A. The output voltage ripples are limited to 10%.

With such values of input and output voltage, we can determine the duty cycle with the relationship below:

$$\alpha = 1 - \frac{V_e}{V_s} \quad (13)$$

According to the values of V_e and V_s, this leads to a duty cycle $\alpha = 0{,}6$.

Current variations in the inductance are tolerated up to 40% and we choose an operating frequency of 47 kHz.

With a desired minimum efficiency of 80%, we can obtain the input current which is also current flowing through the inductor:

$$\frac{P_s}{P_e} = 0{,}8$$

$$I_e = \frac{V_s \times I_s}{0{,}8\, V_e} \quad (14)$$

Numerical application : $I_{emax} = \frac{30\times2}{0.8\times12}$ =6.25A

Our inductor must therefore withstand an intensity of at least 7A; we can then deduce the value of the inductance, knowing the operating frequency:

$$L = \frac{\alpha \times V_e}{f\ \Delta I_e} \quad (15)$$

We have a minimum value of the inductance of:

$$Lm = \frac{\alpha \times V_e}{f\ \Delta I_{emax}} \quad (16)$$

Numerical application : $Lm = \frac{0{,}6\times12}{47\times10^3\times\frac{40\times6.25}{100}}$

$$Lm = 61.27\mu H$$

Any inductance greater than this value will reduce ripple in the input current. In our case, we have chosen a value of 220 µH for a reduction of the current ripple; this value is equally suitable for the duty-cycle selected above but also allows us to go up to the maximum duty-cycle α_max to allow us to draw curves in the second part. Indeed, for this maximum duty cycle, the minimum value of the inductance would be:

$$Lm = \frac{\alpha_{max} \times V_e}{f\ \Delta I_{emax}} \quad (17)$$

Numerical application : $Lm = \frac{12}{47\times10^3\times\frac{40\times6.25}{100}}$

$$Lm = 102.13\ \mu H$$

Thus, the chosen value L = 220 μH covers this eventuality as well. The next step is to determine the value of the capacity to be used.

Since the charge provided by the capacitor is given by : $dQ = \frac{\alpha \times I_s}{f}$, then, we can rewrite :

$$C = \frac{\alpha \times I_s}{f\ \Delta V_s} \quad (18)$$

This expression gives a minimum value of the capacity in the form:

$$C = \frac{\alpha \times I_{smax}}{f\ \Delta V_s} \quad (19)$$

Numerical application: $C = \frac{0{,}6\times2}{47\times10^3\times\frac{10\times30}{100}}$

The minimum capacity value is thus: C=8.51 µF

Any value higher than this will allow us to reduce ripples in the output voltage. We have chosen 470 µF which allows us to minimize output voltage ripples under all operating conditions.

As for the diode used, it must be fast; in fact, losses by reverse overlaps are generated by its diodes, so the faster they are, the less losses there will be. We chose the RHRP15120, which can handle 15A current and 1200V.

The switch we chose must be able to withstand the voltage that will be imposed on it at its terminals, and must also operate at the desired frequency with a low drain-source resistance. One of the reasons for choosing a MOSFET is its operating frequency which exceeds 100kHz. The chosen MOSFET is the 2SK1531. The maximum drain current is 15A, its maximum voltage is 500V and finally its on-state resistance (r_{DSon}) is 0.38 Ω typical.

The control signal for the transistor comes, after opto-isolation by a TLP250, from a Texas Instruments MSP432P401R microcontroller.

The load was chosen so as not to exceed the 2A we set at the output. We used RB58 wound resistors of 47Ω values that hold 11W. So we have mounted two of them in parallel to obtain a load of 23.5 Ω.

The figure below shows the prototype with which the measurements were made.

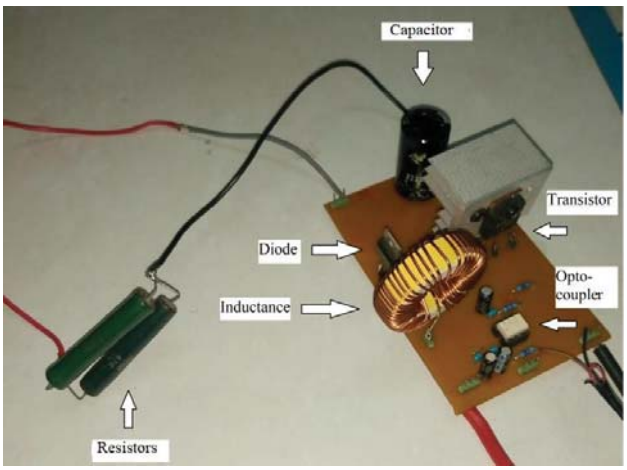

Figure 3- Prototype of the classic boost

b. Visualized signals

The signals were visualized using a two-channel BK PRECISION 2190D 100Mhz oscilloscope. We will thus be able to visualize at best two signals at the same time.

Figure 4 shows the input and output voltages measured at the oscilloscope:

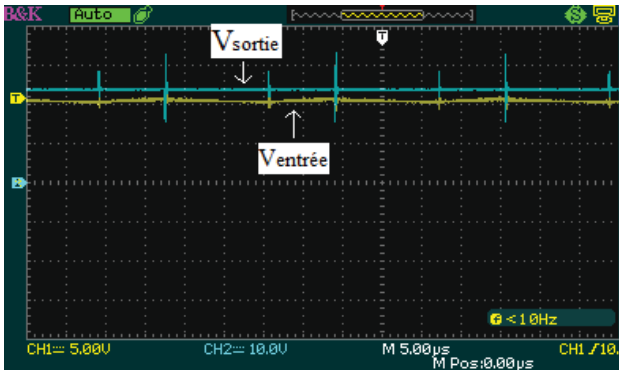

Figure 4- Waveform of boost input and output voltages

The input voltage has some ripples because it is obtained by a switching power supply unit for PC. On the other hand, the output voltage has almost no ripple but there are some peaks due mainly to the parasites coming from the PC power supply used and the fact that we did not add an interference filter at the output of our converter.

The control signal coming from the microcontroller is a square wave signal at constant frequency with a fixed duty cycle; a level adaptation and isolation of the control and the power part were necessary and this is obtained by the TLP250. The signal shapes obtained are shown in the oscillogram in *figure 5*.

The signal coming from the microcontroller rises to about 3.3V and the signal driving the gate of the Mosfet transistor is about 10V, which is more than enough to control the Mosfet transistor.

These two signals are perfectly in phase and the control is effectively carried out with the fixed duty cycle.

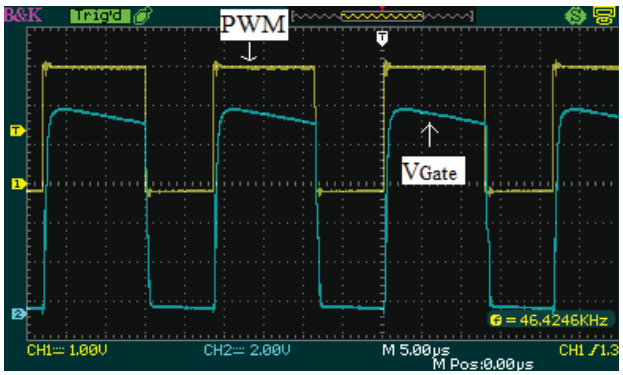

Figure 5- Waveform of the control signal and the V_{GS} voltage of the transistor

After this test of the effective control of the Mosfet transistor, the effective switching of the transistor must be checked as shown in *figure 6*.

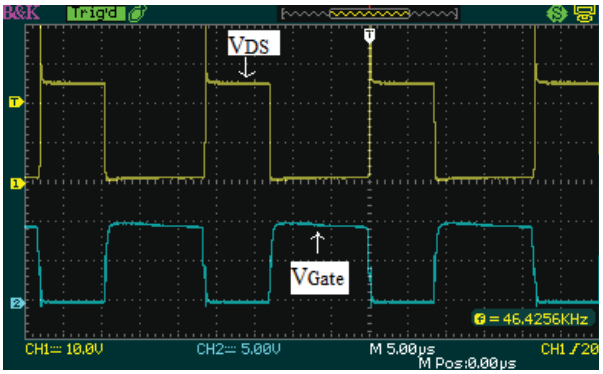

Figure 6- Waveform of the Drain-Source voltage and the Gate voltage of the transistor

The V_{GS} voltage is indeed complementary to the V_{DS} voltage which proves that the transistor really switches.

The test that remains to be done is that of the diode to check how it behaves towards the transistor. This oscillogram is shown in *figure 7*. We can see that the diode voltage in blue is similar to the Drain-Source voltage in yellow (we have the inverse signals here).

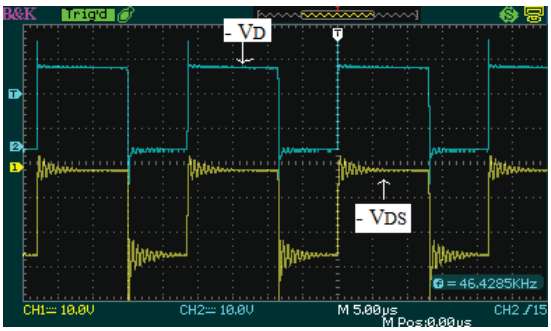

Figure 7- Waveform of the voltage across the diode and the Drain-Source voltage of the transistor

It is therefore complementary to the control signal as well. Indeed, it is null when the diode is conducting and negative when the diode is blocked.

All the signals tested confirm the correct operation of the classic boost; however, before presenting the results obtained for the boost, we present the dimensioning for the quadratic type boost converter.

For the comparison with theoretical model with losses, our dimensioning as presented above was done with maximum duty cycles. This precaution allowed us later, with the same device, to vary the duty cycles and to collect input and output data with voltmeters and amperemeters how we can see in *Figure 8*.

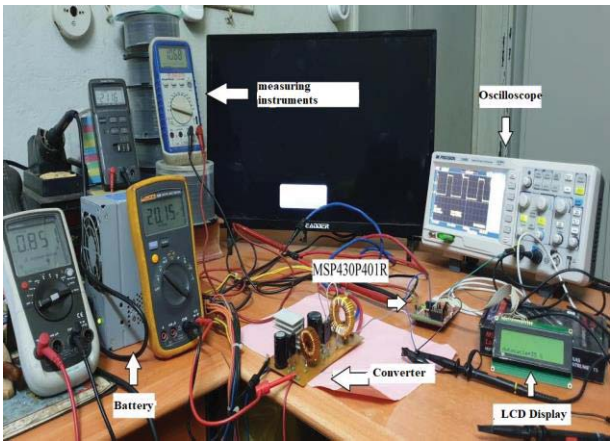

Figure 8 - The experimental system

As said above, we used a transistor that can withstand a high output voltage to hold over a wide range of duty cycles and have a small as possible a r_{DSon}.

III. RESULTS AND DISCUSSION

3.1 Theoretical results

Based on the above mathematical formulation, simulations were performed by varying duty cycle, series resistances, and choosing different transistors and diodes parameters. The effects of the series resistances are pointed out, as well as transistor and diode losses Honadia et al.,2018.

Indeed, we can see in the figures below that the influence of inductive losses is more perceptible when the transistor has a low rdson. It goes without saying that the use of a quality transistor requires, if we want to make it profitable, at least a quality inductance.

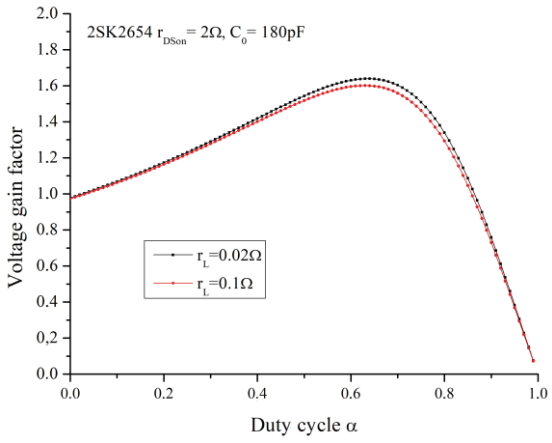

Figure 9-a Voltage gain factor versus duty cycle for 2SK2654

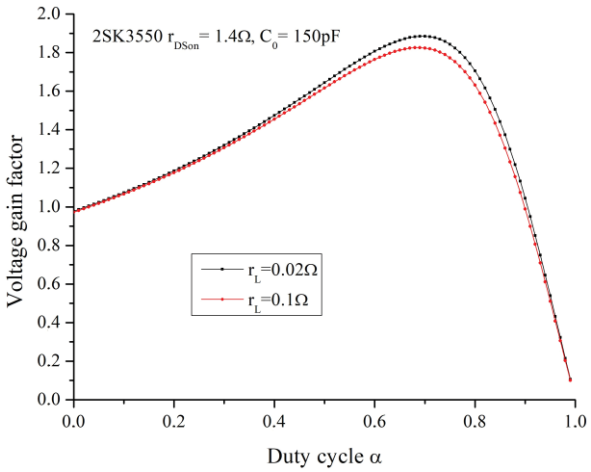

Figure 9-b Voltage gain factor versus duty cycle for 2SK3550

However, even if the r_{DSon} is high, i.e. of the order of one unit, a good choice of inductance allows us to gain 3.3% in voltage in Figure 9-b. Also for r_{DSon} of this order of magnitude, a variation of 0.6 Ω between the transistors of figure 9-a and figure 9-b, allows us to obtain a gain of 15% which is not negligible.

the rdson of the transistors in figure 9-c and figure 9-d below are of the order of one tenth.

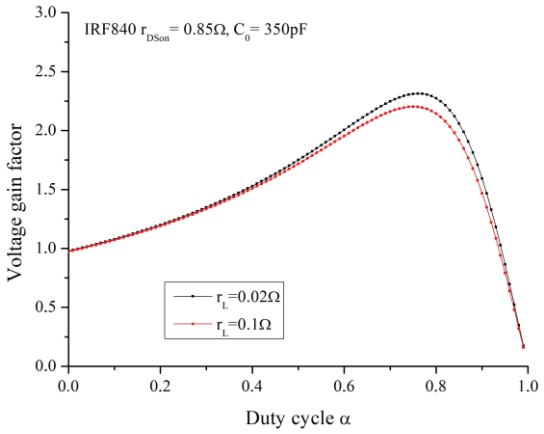

Figure 9-c Voltage gain factor versus duty cycle for IRF840

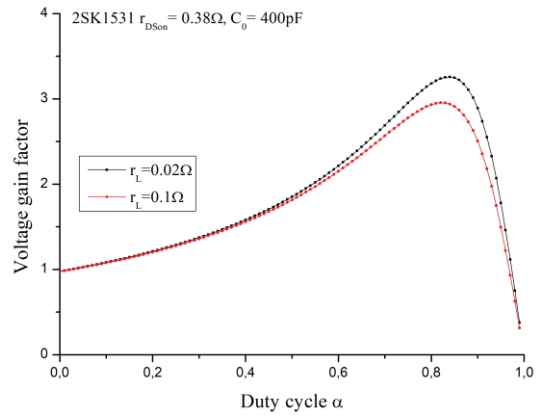

Figure 9-d Voltage gain factor versus duty cycle for 2SK1531

A variation of 0.47 Ω in this case leads to a gain of 40.7%. This is very significant in our context where we must always optimize at the maximum.

The transistors of figure 9-e and figure 9-f have rdson of the order of a hundredth.

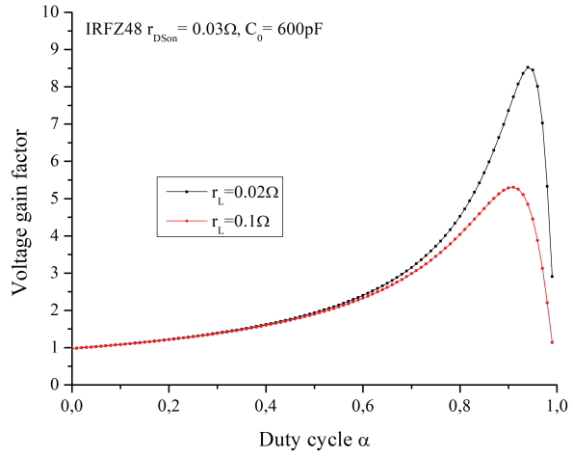

Figure 9-e Voltage gain factor versus duty cycle for IRFZ48

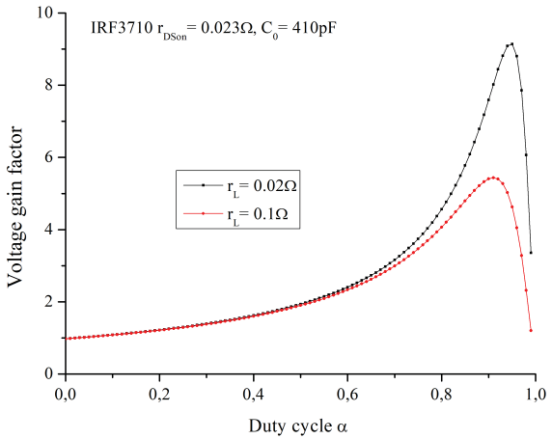

Figure 9-f Voltage gain factor versus duty cycle for IRF3710

The difference between them is only 7 mΩ, but this still results in a gain of 7.3%. When we switch to a transistor that has a r_{DSon} that is of the order of a thousandth like the one in figure 9-g.

In our case, replacing the IRF3710 by the IRF3205 which have a difference of 0.015 Ω, materializing the passage from the hundredth to the thousandth, makes us gain 22.2% on the gain factor.

In the same way by passing from the tenth to the hundredth with the 2Sk1531 and the IRFZ48 which have a difference of 0.35 Ω, we obtain a gain of 61.78%. Also the passage from unity to a tenth is also significant. Indeed, between the 2SK3550 and the IRF840 there is a difference of 0.55Ω at their rdson and this allows us to gain 22.7% on the gain factor.

The same is true for the influence of the r_{DSon}. Indeed, the lower the r_{DSon} is, the steeper the regression slope is, showing an efficiency quite close to unity for a large number of duty cycles.

In general, we can see that more the r_{DSon} are low and the smaller the variations, the greater the impact on both the gain factor and the conversion efficiency.

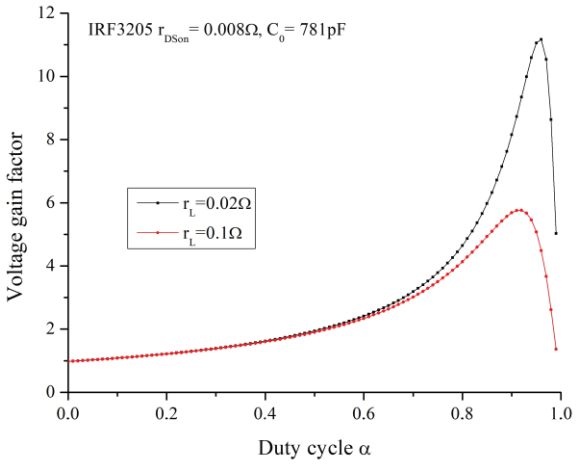

Figure 9-g Voltage gain factor versus duty cycle for IRF3205

The efficiency is a different data from the voltage gain, but we can see in Figures 10 that the resistive losses in the inductor have the same effect; in fact, a good inductor promotes a better conversion efficiency.

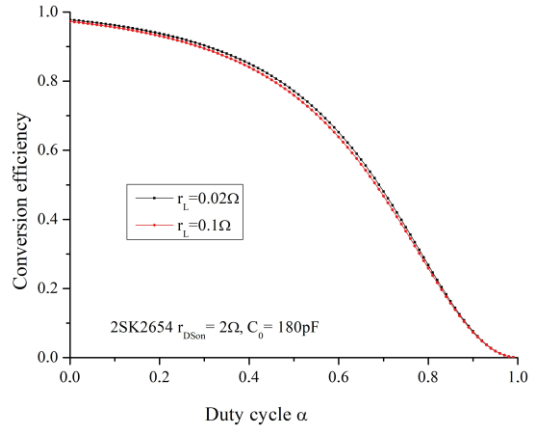

Figure 10-a: Conversion efficiency versus duty cycle for for 2SK2654

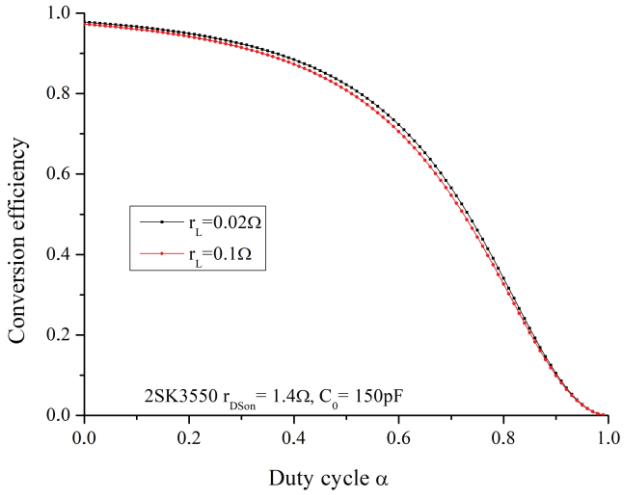

Figure 10-b: Conversion efficiency versus duty cycle for for 2SK3550

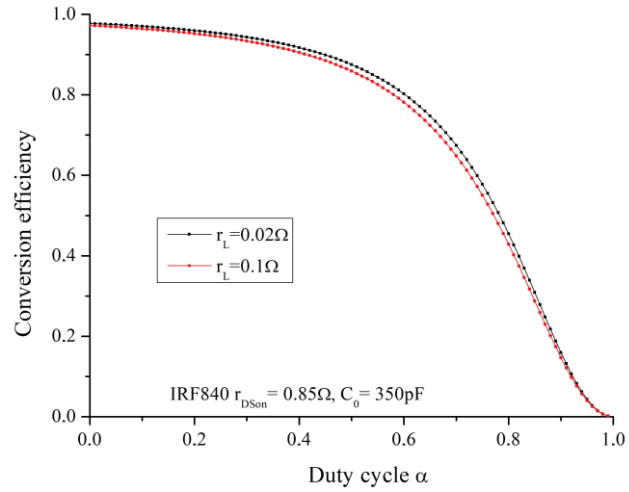

Figure 10-c: Conversion efficiency versus duty cycle for for IRF840

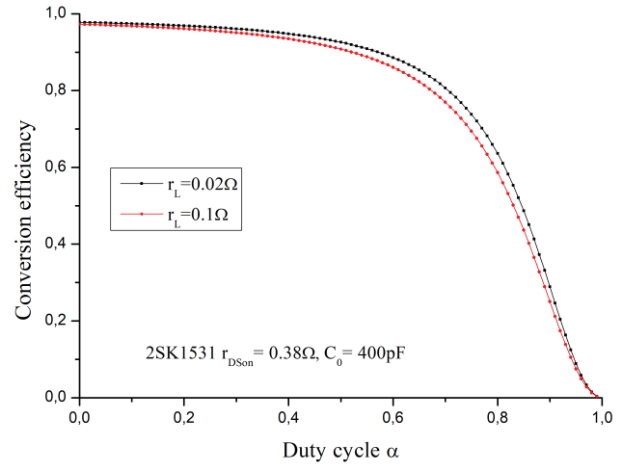

Figure 10-d: Conversion efficiency versus duty cycle for for 2SK1531

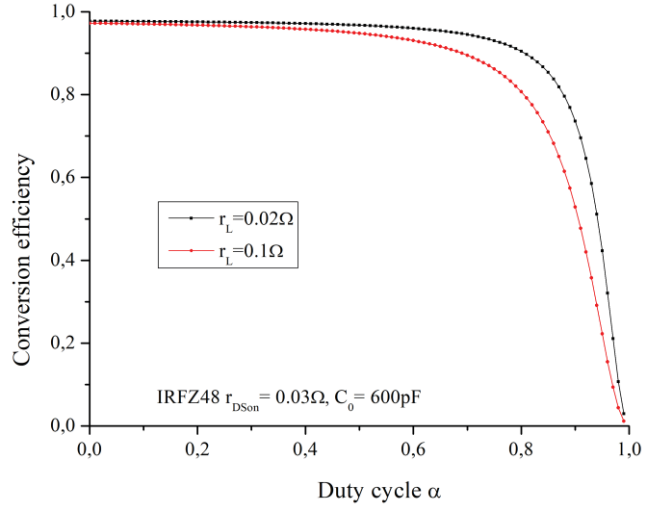

Figure 10-e: Conversion efficiency versus duty cycle for for IRFZ48

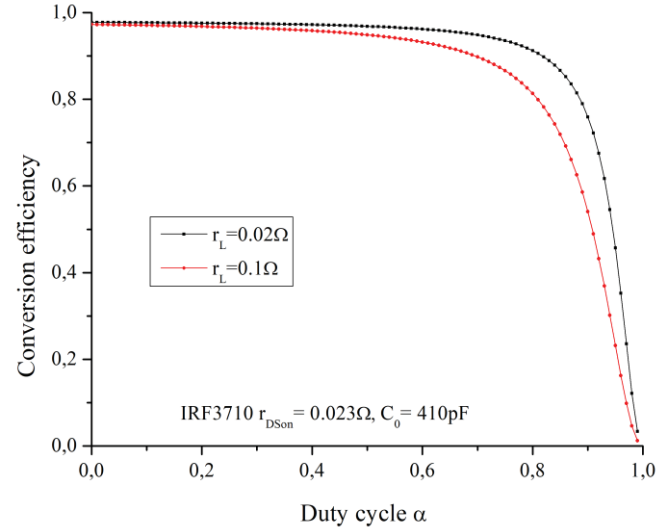

Figure 10-f: Conversion efficiency versus duty cycle for for IRF3710

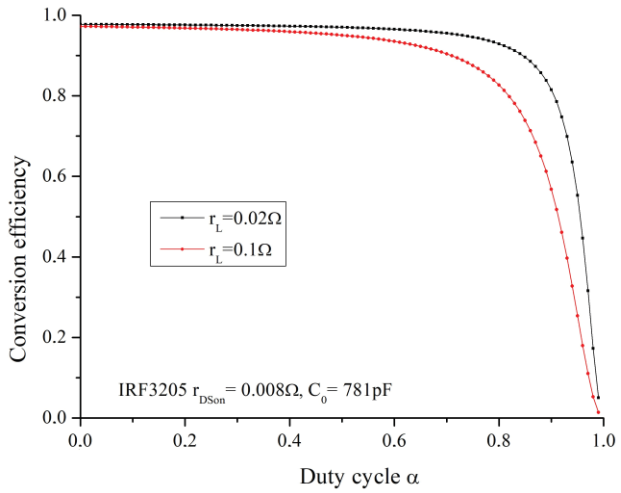

Figure 10-g: Conversion efficiency versus duty cycle for for IRF3205

3.2 Experimental results

Figures 11 and 12 show the ideal, theoretical curves including the real boost parameters and experimental curves for gain and efficiency. The ideal yield, which is unitary, has not been plotted.

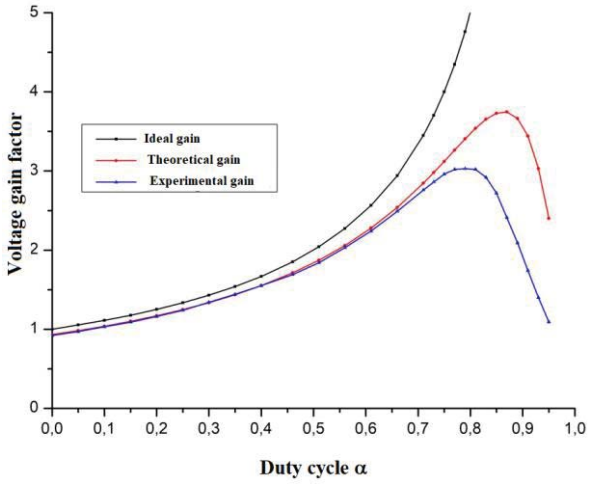

Figure 11 - Comparison between the different voltage gains factors of the boost

In Figure 11, we see that the theoretical and experimental gains gradually diverge from the ideal gain because of the losses that intensify in the converter as the duty cycle increases. These losses are certainly related to the switches that are directly related to the duty cycle. In addition, the Drain-Source Resistance (r_{DSon}) of the transistor and the dynamic voltage (V_F) increase with temperature, thus causing a decrease in converter performance as the converter heats up. This is shown by the divergence of our theoretical gain with the experimental gain for duty cycles higher than 0.7. Indeed, the r_{DSon} being linked to the switching, the more the switching intensifies and the more the r_{DSon} increases leading to a power dissipation which in turn influences the characteristics of the transistor and thus the r_{DSon}. On the other hand, the influence of temperature on the V_F of the diode is less noticeable.

This is confirmed in Figure 12, where the margin of error between theoretical and experimental performance is less than 10% for duty cycles below 0.7; however, this error increases rapidly to values of 50% for higher duty cycles.

Our model is therefore only valid for duty cycles below 0.7. Beyond that, we should be able to introduce the variations with temperature to have a more accurate model.

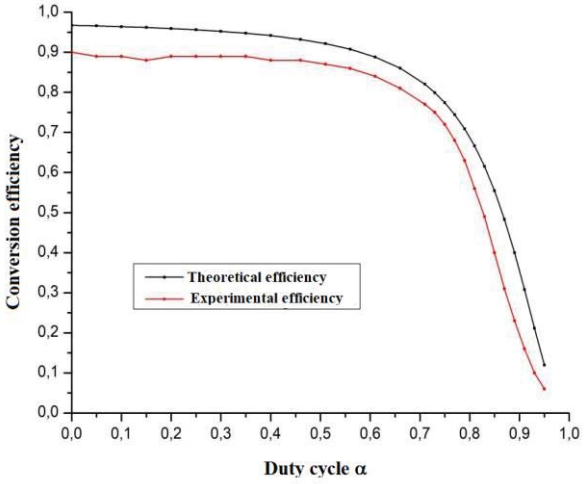

Figure 12- Comparison between the different conversion efficiency of the boost

IV. CONCLUSION

The quality of the components making up a converter plays an important role in the quality of the conversion. Indeed, the deterioration of its components over time will lead to an under-performance of the converter. However, all components do not influence in the same way. The curves previously allowed us to note a priority from the point of view of quality, according to the nature and/or the position, of the component. First we have the active components and then follow the passive components. For the latter type, the influence of the inductance predominates over that of the capacitor. As far as switches are concerned, the influence of the diode is very little felt compared to that of the transistor. Indeed, a transistor with the lowest possible r_{DSon} guarantees a better voltage gain and a better efficiency. However, the r_{DSon} increases with temperature. Indeed, a transistor that will operate at a high duty cycle will overheat faster, which will cause an increase of its r_{DSon} and therefore a decrease of the converter's performance. It is therefore necessary to provide a cooling device if the compromise between r_{DSon} and output voltage does not leave us too much choice. As far as mosfets in general are concerned, the higher the voltage it supports at the output, the higher its r_{DSon} is. A good dimensioning of the transistor according to the needs of the system is therefore imperative.

REFERENCES

Abusorrah, A., Al-Hindawi, M. M., Al-Turki, Y., Mandal, K., Giaouris, D., Banerjee, S., Voutetakis, S. and Papadopoulou, S. (2013) Stability of a boost converter fed from photovoltaic source, Solar Energy, 98, 458-471. https://doi.org/10.1016/j.solener.2013.09.001

Ayop, R. and Tan, C. W. (2018) Design of boost converter based on maximum power point resistance for photovoltaic applications, Solar Energy, 160, 322–335. https://doi.org/10.1016/j.solener.2017.12.016

Branko L. Dokić, Branko Blanuša, (2015) Power Electronics: Converters and Regulators, 3rd Edition, Springer International Publishing.

Das, M., Agarwal, V. (2012) A novel, high efficiency, high gain, front end dc-dc converter for low input voltage solar photovoltaic applications, Proceedings of the 38th Annual Conference of the IEEE IECON, 5744–5749.

Dash, S. S. and Nayak, B. (2015) Control analysis and experimental verification of a practical dc–dc boost converter, Journal of Electrical Systems and Information Technology, 2, 378-390. https://doi.org/10.1016/j.jesit.2015.08.001

Durán, E., Andújar, J. M., Segura, F., Barragán, A. J. (2011) A high-flexibility DC load for fuel cell and solar arrays power sources based on DC–DC converters, Applied Energy, 88, 1690-1702. https://doi.org/10.1016/j.apenergy.2010.11.002

Erickson, R.W., Maksimovic, D. (2004) Fundamentals of power electronics. 2nd Edition, New York, Kluwer Academic Publishers.

Haibing, H., Qian, Z., Xiang, F., Shen, Z. J. and Batarseh, I. (2011) A single stage mi-cro-inverter based on a three-port flyback with power decoupling capability. Energy Conversion Congress and Exposition (ECCE), IEEE, 1411-1416.

Honadia, P.A.A., Barro, F.I. and Sané, M. (2018) Performance Analysis of a Boost Converter with Components Losses. Energy and Power Engineering, 10, 399-413. https://doi.org/10.4236/epe.2018.109025

Kesraoui, M., Korichi, N. and Belkadi, A. (2011) Maximum power point tracker of wind energy conversion system. Renew Energy; 36, 2655-2662. https://doi.org/10.1016/j.renene.2010.04.028

Li, Q. and Wolfs, P. (2008) A Review of the Single Phase Photovoltaic Module Integrated Converter Topologies With Three Different DC Link Configurations. IEEE Trans. on Power electron. 23, 320-1333.

Li, W., Lv, X., Deng, Y., Liu, J. and He, X. (2009) A Review of Non-Isolated High Step-Up DC/DC Converters in Renewable Energy Applications, 24th Annual Conference and Exposition of the IEEE, Applied Power Electronics Conference and Exposition, Washington DC, 15-19 February 2009,364-369.

Mahela, O. P., Shaik, A. G. (2017) Comprehensive overview of grid interfaced solar pho-tovoltaic systems, Renewable and Sustainable Energy Reviews, 68, 316-332. https://doi.org/10.1016/j.rser.2016.09.096

Petreuş, D., Daraban, S., Ciocan, I., Patarau, T., Morel, C. and Machmoum, M. (2013) Low cost single stage micro-inverter with MPPT for grid connected applications, Solar Energy, 92, 241-255. https://doi.org/10.1016/j.solener.2013.03.016

Rajesh, R., Mabel, M. C. (2015) A comprehensive review of photovoltaic systems, Re-newable and Sustainable Energy Reviews, 51, 231-248. https://doi.org/10.1016/j.rser.2015.06.006

Sadek, U., Sarjaš, A., Svečko, R., Chowdhury, A. (2015) FPGA-based control of a DC-DC boost converter, IFAC-PapersOnLine, 48, 22-27. https://doi.org/10.1016/j.ifacol.2015.08.102

Shuhui, L., Timothy, A. H. and Dawen, L. (2011) Fei H. Integrating photovoltaic and power converter characteristics for energy extraction study of solar PV systems. Renew Energy; 36, 3238-45. https://doi.org/10.1016/j.renene.2011.02.016

Taghvaee, M. H., Radzi, M. A. M., Moosavain, S. M., Hizam, H. and Marhaban, M. H. (2013) A current and future study on non-isolated DC–DC converters for photovoltaic applications, Renewable and Sustainable Energy Reviews, 17, 216–227. https://doi.org/10.1016/j.rser.2012.09.023

Ternifi, Z. E. T., Petit, P., Bachir, G. and Aillerie, M. (2017) New Topology of Photovoltaic Microinverter based on Boost converter. Energy Procedia, 119, 938-944. https://doi.org/10.1016/j.egypro.2017.07.106

Variath, R. C., Andersen, M. A. E., Nielsen O. N. and A. Hyldgard. (2010) A review of module inverter topologies suitable for photovoltaic systems. Proc. IEEE IPEC, 310-316.

Wang, T. and Tang, Y. (2013) A High Step-up Voltage Gain DC/DC Converter for the Micro-Inverter. IEEE 8th Conference on Industrial Electronics and Applications (ICIEA), 1089-1094.

Winder, S. (2017) Power Supplies for LED Driving, 2nd Edition, Newnes.

Wu, G., Ruan, X. and Ye, Z. (2018) Non-isolated high step-up DC–DC converter adopting auxiliary capacitor and coupled inductor, J. Mod. Power Syst. Clean Energy, 6, 384–398. https://doi.org/10.1007/s40565-017-0342-8

Wu, K. (2016) Power Converters with Digital Filter Feedback Control, Academic Press.

Wu, K. C. (1997) Pulse Width Modulated DC-DC Converters, Springer US, 1997. https://doi.org/10.1007/978-1-4615-6021-0

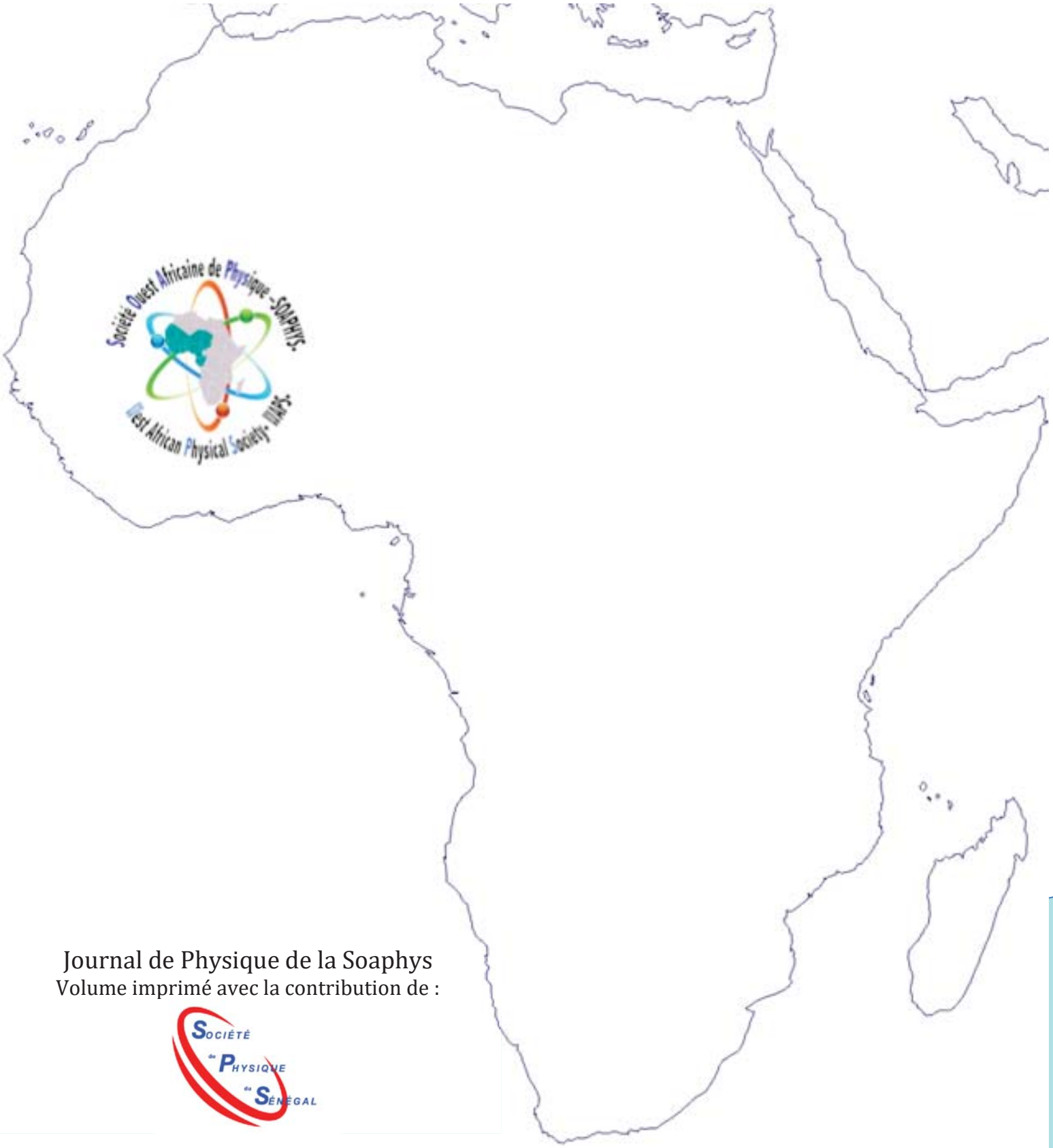

Journal de Physique de la Soaphys

Volume imprimé avec la contribution de :